Engineering Spin Waves in a High-Spin Ultracold Fermi Gas

J. Heinze,[1] J. S. Krauser,[1] N. Fläschner,[1] K. Sengstock,[1,2,*] and C. Becker[1,2]

[1]*Institut für Laser-Physik, Universität Hamburg, Luruper Chaussee 149, 22761 Hamburg, Germany*
[2]*Zentrum für Optische Quantentechnologien, Universität Hamburg, Luruper Chaussee 149, 22761 Hamburg, Germany*

U. Ebling,[3] A. Eckardt,[4] and M. Lewenstein[3,5]

[3]*ICFO-Institut de Ciències Fotòniques, Avenida Carl Friedrich Gauss, 3, 08860 Castelldefels (Barcelona), Spain*
[4]*Max-Planck-Institut für Physik komplexer Systeme, Nöthnitzer Straße 38, 01187 Dresden, Germany*
[5]*ICREA-Institució Catalana de Recerca i Estudis Avançats, Lluís Companys 23, 08010 Barcelona, Spain*
(Received 18 February 2013; published 19 June 2013)

We report on the detailed study of multicomponent spin waves in an $s = 3/2$ Fermi gas where the high spin leads to novel tensorial degrees of freedom compared to $s = 1/2$ systems. The excitations of a spin-nematic state are investigated from the linear to the nonlinear regime, where the tensorial character is particularly pronounced. By tuning the initial state we engineer the tensorial spin-wave character, such that the magnitude and the sign of the counterflow spin currents are effectively controlled. A comparison of our data with numerical and analytical results shows good agreement.

Spin-interaction driven phenomena are crucial for the behavior of many quantum systems, e.g., ferromagnets [1] and high-temperature superconductors [2] and they are also relevant in spintronics applications [3]. Apart from condensed matter systems with an electronic spin of $s = 1/2$, dilute atomic gases show a wealth of novel spin excitations, where the spin is provided by the internal hyperfine structure of the atoms. Pioneering experiments with hydrogen [4] and helium [5] showed the existence of transverse spin waves, which arise from intrinsic spin-exchange interactions [6–8]. Longitudinal spin waves in two-component mixtures have been observed in noncondensed bosonic ^{87}Rb gases [9–11]. For weakly interacting fermions, slow spin currents were reported near the zero crossing of a Feshbach resonance [12–14] and the interaction-induced damping of dipole oscillations was studied [15]. Prominent examples for spin-dependent phenomena in strongly interacting fermionic systems are the miscibility of spin mixtures [16] and the quest for itinerant ferromagnetism [17–20]. In contrast to conventional two-component systems, the hyperfine structure of many atoms also allows for spinor gases with $s > 1/2$, which offer a whole new set of possibilities to study spin-dependent phenomena [21–24]. This includes spin-changing collisions [25,26], hidden interaction symmetries [27,28], spontaneous domain formation [29], the existence of spin-nematic states [30,31], novel superfluid phases [32,33], and SU(N) degenerate ground states [34–38]. For fermionic atoms, $s = 3/2$ constitutes the simplest realization of a high-spin system and has been thoroughly studied theoretically, being a model system for all higher spins [27,28,39].

In this Letter, we demonstrate the controlled generation of spin waves in a quantum degenerate Fermi gas with pseudospin $s = 3/2$. We experimentally study the properties of these fundamental collective spin excitations for a wide range of parameters. The results are explained within a generalized semiclassical mean-field theory (SMFT) for fermionic atoms with a high spin of $s \geq 3/2$, which is an extension of the collisionless Boltzmann equation used to describe conventional $s = 1/2$ systems [7,13,14,40,41]. Spin waves in such high-spin systems are predicted to exhibit very complex and novel properties, which can be most intuitively understood in the language of irreducible spherical tensors (for bosonic gases, see [42,43]). While for $s = 1/2$ it is sufficient to use the identity and the three spin matrices [12], the description of higher spins additionally requires higher-order tensors, such as the nematic and octupole tensor for $s = 3/2$.

We have investigated spin-wave excitations from the linear regime, where the oscillation frequency is minimal, to the nonlinear regime, where the spin-wave frequency strongly depends on the excitation amplitude. The use of the tensor basis allows us to directly observe the effect of the nonlinear mode coupling, which leads to the excitation of breathing modes in the spin-nematic component. Moreover, we demonstrate the controlled manipulation of the spin-wave composition by engineering the coherences of the initial state. In that way, the spin current for two of the four components can be reversed changing the spin-wave character from spin octupole to spin vector. Our results illustrate the high degree of control that can be exerted on spin waves in high-spin Fermi gases. The good agreement with the theoretical results shows that our SMFT well describes high-spin Fermi gases in the quantum degenerate regime. The combined experimental and theoretical findings pave the way toward novel schemes for atom spintronics using the intrinsic high spin.
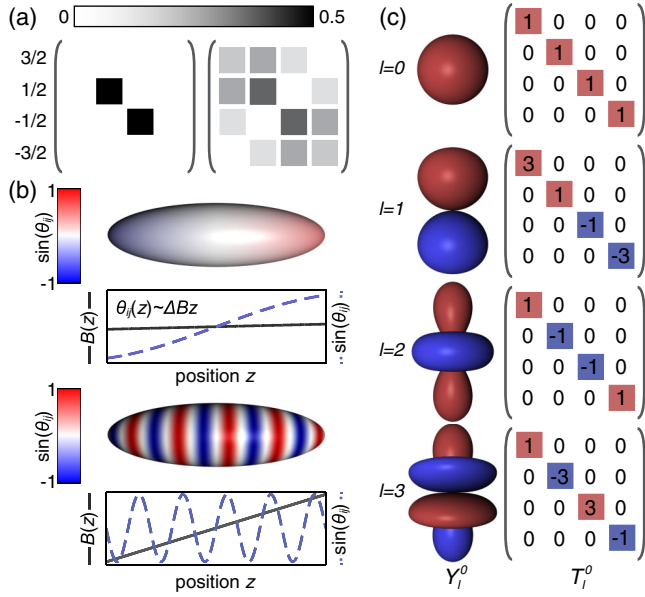
FIG. 1 (color online). (a) Single-particle density matrix for an incoherent superposition of $|1/2\rangle$ and $|-1/2\rangle$ (left) and the resulting coherent superposition of all four components after a resonant rf pulse (right). Diagonal elements W_{ii} are real and represent the populations. Off-diagonal elements are complex numbers $W_{ij} = |W_{ij}|e^{i\theta_{ij}}$ and include the phase θ_{ij} between different components. Only the absolute value $|W_{ij}|$ is plotted. (b) Sketch of the local phase across the Fermi gas after pulses with different magnetic field gradients. (c) $m = 0$ component of the $l = 0, 1, 2, 3$ tensor operators T_l^m for $s = 3/2$ in comparison to the corresponding spherical harmonics Y_l^m.

FIG. 2 (color online). (a) *In situ* time evolution of all four spin components after a 10 ms pulse with a magnetic field gradient of $\Delta B = 3.4$ G/m. Shown are the column densities at different times after the excitation. (b) Deviation from the initial population of the $m = 0$ component of the vector ($l = 1$), nematic ($l = 2$), and octupole ($l = 3$) components. The vector and octupole components show spatial dipole oscillations, while the nematic component clearly exhibits breathing dynamics. (c),(d) Numerical calculation for the parameters of (a),(b).

Our measurements are performed in a quantum degenerate gas of ^{40}K in the $f = 9/2$ hyperfine manifold. We initially evaporate a balanced mixture of $|m = 1/2\rangle$ and $|m = -1/2\rangle$ to quantum degeneracy in an elongated, spin-independent optical dipole trap [40]. The final trapping frequencies are $\omega_{x,y,z} = 2\pi \times (70, 70, 12)$ Hz. At this point, we apply a radio-frequency (rf) pulse to create a coherent superposition with the states $|\pm 3/2\rangle$ [Fig. 1(a)]. We initialize the spin waves by applying a small magnetic field gradient up to a few G/m for 10 ms, which leads to a phase spiral for coherent superpositions of different spin components as sketched in Fig. 1(b). While these coherent superpositions are initially still spin polarized locally, the phase twist allows for interactions in a trapped gas where the external potential induces spatial dynamics [41]. In general, the resulting mean-field interaction couples the spin degrees of freedom to different modes of the external trap leading to the emergence of spin waves. We detect the spin current using absorption imaging either *in situ* or after 18.5 ms time of flight (TOF) with a Stern-Gerlach separation of the spin components [40]. In Fig. 2(a) we show a typical example for an $s = 3/2$ spin wave initialized by a 10 ms gradient of $\Delta B = 3.4$ G/m. The measurements reveal oscillatory spin currents in all four spin components.

We observe a time-independent total density, meaning that the spin waves constitute counterflow spin currents without an accompanying net mass transport. In particular, note the inverted flow direction of $|1/2\rangle$ ($|-1/2\rangle$) with respect to $|3/2\rangle$ ($|-3/2\rangle$), which is a clear indication of the new tensorial degrees of freedom as discussed later.

For the theoretical description of high-spin Fermi gases, we generalize a one-dimensional SMFT [40] previously used to explain spin-wave phenomena in thermal fermionic and bosonic systems with effective spin 1/2 [7,10,11,13,14,41] and to predict the spin-wave dynamics in thermal bosonic $s = 1$ gases [42,43]. The multicomponent system is described in a mean-field fashion by a single-particle density matrix (SPDM) in the form of a one-dimensional Wigner function $W_{kl}(z, p)$ with spin indices k and l. The semiclassical equations of motion take the form of a Boltzmann equation in the collisionless regime. To leading order they read

$$\partial_t W(z, p) = \partial_0 W(z, p) + \frac{1}{i\hbar}[W(z, p), V(z)], \quad (1)$$

assuming a spin-independent external harmonic trap. Here, $V_{mn}(z) = \int \sum_{kl}(U_{klnm} - U_{kmnl})W_{kl}(z, p)dp$ is the effective mean-field potential with the spin-dependent coupling

constants U_{ijkl} [40], $\partial_0 = (-p/m\partial_z + m\omega_z^2 z\partial_p)$ captures the time evolution due to the harmonic trap and the kinetic energy, m is the mass of ^{40}K, and $[.,.]$ indicates the commutator in spin space. In the simulations, higher-order terms of the mean-field interactions are also taken into account, leading to very small deviations only [40]. For an $s = 3/2$ system, the Wigner function in spin space is a 4×4 SPDM, where the diagonal elements W_{ii} represent the absolute population of the spin components and the off-diagonal elements $W_{ij} = |W_{ij}|e^{i\theta_{ij}}$ represent the single-particle coherences between different components. To induce a time evolution of the populations W_{ii}, it is sufficient to spatially vary the phases θ_{ij} of the off-diagonal elements W_{ij}, since both are coupled via the commutator in Eq. (1). Figure 2(c) shows numerical results for the exact experimental parameters, which are in good agreement with the measured results. This demonstrates the capability of the SMFT to quantitatively describe interacting high-spin Fermi gases in the quantum degenerate regime.

To obtain deeper insight into the underlying physical processes, let us at this point briefly recall the description of spin in the language of irreducible spherical tensors T_l^m, which simplify the equations of motion drastically. The T_l^m transform invariantly under rotations and therefore can be ordered by a total spin l and a magnetic quantum number $m = -l, \ldots, l$. Most common are the spherical harmonics for orbital angular momentum [Fig. 1(c)] and the spin vector $\vec{S} \propto (\sigma_x, \sigma_y, \sigma_z)$ where σ_i are the Pauli matrices. Decomposing the Wigner function (mean field) in the tensor basis as $W_l^m = \mathrm{Tr}(T_l^m W)$ [$V_l^m = \mathrm{Tr}(T_l^m V)$], the $m = 0$ components describe the occupations whereas all other components describe coherences. Any (pseudo) $s = 1/2$ system can be conveniently described by the identity matrix ($l = 0$) describing the total density, and the spin vector $\vec{S}$ ($l = 1$) describing the magnetization and the coherences [11–14,41]. To describe the physics of larger spins it is necessary to include higher-order tensors. In a spin $3/2$ system, as discussed here, the spin-nematic tensor ($l = 2$) and the spin-octupole tensor ($l = 3$) must be included (see Fig. 1(c) and [40]).

Figures 2(b) and 2(d) show the time evolution of the $m = 0$ component of the $l = 1, 2, 3$ tensors for the experimental and numerical data of Figs. 2(a) and 2(c), respectively. Note the predominantly breathing dynamics of the spin-nematic component, which is qualitatively different from the spatial dipole oscillations in the spin-vector and spin-octupole components. This results from a linear decoupling of the nematic component due to the rotational symmetry which can be understood by inserting the decomposition W_l^m (V_l^m) into Eq. (1). The rotational symmetry of the interactions leads to the particular simplification that $V_l^m \propto W_l^m$. Omitting the m index for simplicity the equations of motion read [44]

$$\partial_t W_0 \cong \partial_0 W_0,$$

$$\partial_t W_1 \cong \partial_0 W_1 + \frac{1}{i\hbar}([W_1, V_1] + [W_2, V_2] + [W_3, V_3]),$$

$$\partial_t W_2 \cong \partial_0 W_2 + \frac{1}{i\hbar}([W_2, V_1 + V_3] + [W_1 + W_3, V_2]),$$

$$\partial_t W_3 \cong \partial_0 W_3 + \frac{1}{i\hbar}([W_3, V_1] + [W_1 + W_3, V_3] + [W_2, V_2]).$$

(2)

The structure of Eqs. (2) together with the relation $V_l^m \propto W_l^m$ has several important consequences. First, the total density W_0^0 is not altered by the phase spiral, since its time derivative does not depend on the off-diagonal elements; it remains constant as we observed in the experiment. Second, the time derivative of the nematic tensors W_2^m is proportional to the vector and octupole components (W_1^m and W_3^m), but does not depend on a term $[W_2^m, V_2^m]$. This is a result of time-reversal symmetry and leads to a linear decoupling of the nematic component, in the sense that a purely nematic state does not support nematic excitations to first order. In the nonlinear regime, however, where vector and octupole excitations possess a large amplitude, nematic excitations are created via nonlinear mode coupling. This leads to the weak breathing dynamics of the nematic component visible in Fig. 2, where a purely nematic state was initially prepared. The discussion above demonstrates the improved insight into high-spin spin waves granted by the irreducible spherical tensor description.

To analyze the behavior of the system for different excitation amplitudes, we applied different gradient strengths during the initialization of the spin wave [45]. This corresponds to a change of the initial phases θ_{ij} in the SPDM, while the initial coherence amplitudes $|W_{ij}|$ are kept constant. In Fig. 3 experimental results are compared to numerical calculations and show good agreement: For small gradients, the frequency is amplitude-independent and the amplitude rises approximately linearly with the gradient strength. For large gradients, the frequency approaches the trapping frequency and is again only weakly dependent on the excitation amplitude. For intermediate gradients, the system shows a strongly nonlinear behavior which results in an amplitude-dependent oscillation frequency. In the regime of small gradients, corresponding to small excitation strengths one can linearize Eqs. (2) and describe excitations in terms of their leading moments in z and p [10], which corresponds to pure spatial dipole oscillations [40]. Their oscillation frequency for the present initial state can be derived to be $\omega = \sqrt{\omega_{\mathrm{mf}}^2 + \omega_z^2} - \omega_{\mathrm{mf}}$, where ω_{mf} is the mean-field interaction energy as defined in Ref. [40]. This frequency is determined by a competition between the trap-induced spatial oscillations and the mean-field induced rotation of the spin. For our parameters, we calculate
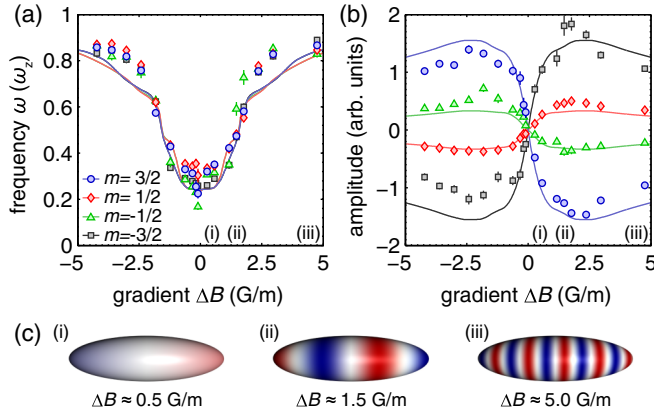
FIG. 3 (color online). (a) Frequency and (b) oscillation amplitude of spin waves excited with different magnetic field gradients at $\omega_z = 12$ Hz. Negative amplitudes denote an inverted initial direction. Solid lines are numerical data for each component. All error bars solely correspond to fit errors, representing one standard deviation. The experimental amplitudes which are taken after TOF and the numerical amplitudes calculated *in situ* are rescaled onto each other by a global factor. (c) Sketch of the phase windings across the atom cloud for different gradient pulses, as indicated by labels (i), (ii) and (iii) in (a) and (b).

$\omega = 2\pi \times 2.3$ Hz, which is in good agreement with the experimental results. The linearized equations of motion also confirm the pure vector and octupole character of the dipole excitations for a perfectly nematic initial state as discussed above. For large gradients, the frequency slowly approaches the trapping frequency: In this regime, the phase spiral is averaged out dynamically on time scales $2\pi/\omega_z$ [41] such that the mean-field potential no longer affects the subsequent oscillation.

All measurements discussed so far were performed with the same purely nematic initial state. By modifying the rf-pulse sequences used for the preparation of the initial state we can control the amplitude of the coherences $|W_{ij}|$ and populations W_{ii} in the SPDM. By this the multipole decomposition of the initial state can be widely controlled and allows for the initialization of, e.g., pure vector or nematic initial states, which in turn results in different spin and spatial characteristics of the emerging spin wave. Following this direction, we performed a second set of experiments, where we engineered the spin-wave excitations by keeping the population of all four spin components constant but changing the initial coherence amplitudes $|W_{ij}|$ [Fig. 4(b)]. Note, that this is complementary to the results shown in Fig. 3, where we changed the phase θ_{ij} of the coherence by using different gradient strengths. Figure 4(a) shows the resulting oscillation amplitude for all four spin components depending on $c = |W_{1/2,-1/2}/W_{1/2,1/2}|$. At $c \approx 0.5$, the system changes its qualitative behavior where the $|\pm 1/2\rangle$ components interchange their oscillation direction. Using the tensor notation, the spin wave at small c is dominated by the
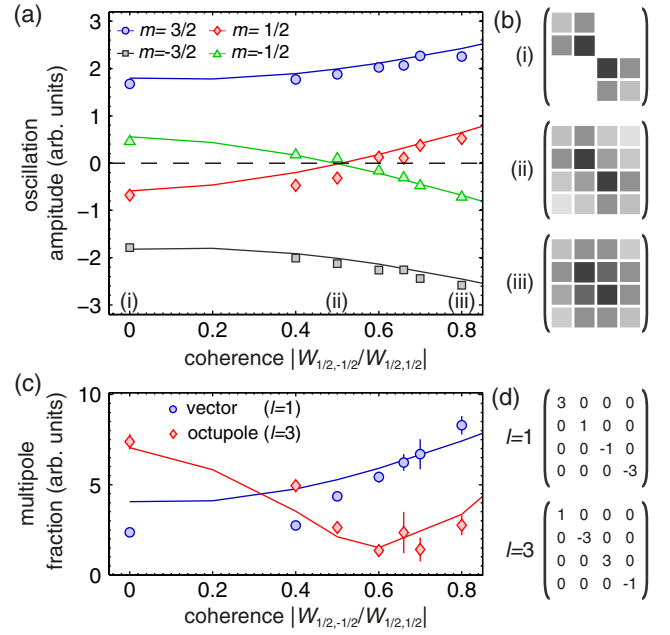
FIG. 4 (color online). (a) Spatial oscillation amplitude of the spin-wave excitations for different initial coherences but equal populations of the four components at $\Delta B = 3.6$ G/m. Solid lines show the initial spin-wave amplitude extracted from numerical calculations. (b) Exemplary SPDMs for different initial coherences as indicated by labels (i), (ii) and (iii) in (a). (c) Amplitude of the dipole and octupole tensor components [40]. (d) Vector and octupole tensors evaluated in (c). All error bars solely correspond to fit errors, representing one standard deviation. The experimental amplitudes which are taken after TOF and the numerical amplitudes calculated *in situ* are rescaled onto each other by a global factor.

spin octupole, where neighboring spin components have an inversed sign and therefore oscillate in opposed directions. At large c, the oscillation becomes spin-vector dominated, where spin components with the same sign of magnetization oscillate in the same direction [Fig. 4(c)]. The anew increase of the octupole amplitude at large c is due to higher-order spatial excitations, possible in the nonlinear regime, where the measurements were performed. At $c \approx 0.5$, the vector and octupole component contributions mutually cancel each other, leading to a vanishing spin current in the $|\pm 1/2\rangle$ components. Again the numerical calculations describe the engineered spin waves very well.

In conclusion, we have thoroughly investigated the physics of collective spin waves in a high-spin Fermi gas. Comparing experimental and numerical results, we showed that high-spin Fermi gases in the quantum degenerate regime can be well described using a SMFT. We have analyzed the spin-wave excitation spectrum for different excitation strengths ranging from the linear deep into the nonlinear regime. By employing irreducible spherical tensors, the SMFT allows us to intuitively explain the novel emerging spin-wave characteristics in a high-spin system. We find a linear decoupling of the spin-nematic

component, which in turn allowed us to directly observe nonlinear mode coupling in the spin-wave dynamics. Finally, we demonstrated how to control the multipole character of spin waves which leads to a reversal of the resulting counterflow spin current of two spin components. Our results constitute the first experimental investigation of coherent many-body dynamics of a high-spin fermionic quantum gas. They demonstrate the controlled manipulation of atomic spin currents which, together with the theoretical understanding, paves the way toward novel schemes for spintronics in ultracold atomic gases, using the intrinsic high spin as a valuable resource.

———————

*Corresponding author.
klaus.sengstock@physnet.uni-hamburg.de

[1] D. Vollhardt, N. Blumer, K. Held, and M. Kollar, *Metallic Ferromagnetism: An Electronic Correlation Phenomenon*, Lecture Notes in Physics Vol. 580 (Springer, Heidelberg, 2001).

[2] P. A. Lee, N. Nagaosa, and X.-G. Wen, Rev. Mod. Phys. **78**, 17 (2006).

[3] I. Žutić, J. Fabian, and S. Das Sarma, Rev. Mod. Phys. **76**, 323 (2004).

[4] B. R. Johnson, J. S. Denker, N. Bigelow, L. P. Lévy, J. H. Freed, and D. M. Lee, Phys. Rev. Lett. **52**, 1508 (1984).

[5] W. J. Gully and W. J. Mullin, Phys. Rev. Lett. **52**, 1810 (1984).

[6] E. P. Bashkin, JETP Lett. **33**, 8 (1981).

[7] C. Lhuillier and F. Laloë, J. Phys. **43**, 197 (1982).

[8] L. P. Lévy and A. E. Ruckenstein, Phys. Rev. Lett. **52**, 1512 (1984).

[9] J. M. McGuirk, H. J. Lewandowski, D. M. Harber, T. Nikuni, J. E. Williams, and E. A. Cornell, Phys. Rev. Lett. **89**, 090402 (2002).

[10] T. Nikuni, J. E. Williams, and C. W. Clark, Phys. Rev. A **66**, 043411 (2002).

[11] J. N. Fuchs, D. M. Gangardt, and F. Laloë, Eur. Phys. J. D **25**, 57 (2003).

[12] X. Du, L. Luo, B. Clancy, and J. E. Thomas, Phys. Rev. Lett. **101**, 150401 (2008).

[13] F. Piéchon, J. N. Fuchs, and F. Laloë, Phys. Rev. Lett. **102**, 215301 (2009).

[14] S. S. Natu and E. J. Mueller, Phys. Rev. A **79**, 051601(R) (2009).

[15] B. DeMarco and D. S. Jin, Phys. Rev. Lett. **88**, 040405 (2002).

[16] A. Sommer, M. Ku, G. Roati, and M. W. Zwierlein, Nature (London) **472**, 201 (2011).

[17] G. B. Jo, Y. R. Lee, J. H. Choil, C. A. Christensen, T. H. Kim, J. H. Thywissen, D. E. Pritchard, and W. Ketterle, Science **325**, 1521 (2009).

[18] S. Zhang and T. L. Ho, New J. Phys. **13**, 055003 (2011).

[19] G. J. Conduit and E. Altman, Phys. Rev. A **83**, 043618 (2011).

[20] D. Pekker, M. Babadi, R. Sensarma, N. Zinner, L. Pollet, M. W. Zwierlein, and E. Demler, Phys. Rev. Lett. **106**, 050402 (2011).

[21] T. L. Ho, Phys. Rev. Lett. **81**, 742 (1998).

[22] C. K. Law, H. Pu, and N. P. Bigelow, Phys. Rev. Lett. **81**, 5257 (1998).

[23] T. Ohmi and K. Machida, J. Phys. Soc. Jpn. **67**, 1822 (1998).

[24] T. L. Ho and S. Yip, Phys. Rev. Lett. **82**, 247 (1999).

[25] J. Stenger, S. Inouye, D. M. Stamper-Kurn, H.-J. Miesner, A. P. Chikkatur, and W. Ketterle, Nature (London) **396**, 345 (1998).

[26] J. S. Krauser, J. Heinze, N. Fläschner, S. Götze, O. Jürgensen, D.-S. Lühmann, C. Becker, and K. Sengstock, Nat. Phys. **8**, 813 (2012).

[27] C. Wu, J. P. Hu, and S. C. Zhang, Phys. Rev. Lett. **91**, 186402 (2003).

[28] C. Wu, Mod. Phys. Lett. B **20**, 1707 (2006), and references therein.

[29] L. E. Sadler, J. M. Higbie, S. R. Leslie, M. Vengalattore, and D. M. Stamper-Kurn, Nature (London) **443**, 312 (2006).

[30] R. B. Diener and T. L. Ho, Phys. Rev. Lett. **96**, 190405 (2006).

[31] R. Barnett, A. Turner, and E. Demler, Phys. Rev. Lett. **97**, 180412 (2006).

[32] P. Lecheminant, E. Boulat, and P. Azaria, Phys. Rev. Lett. **95**, 240402 (2005).

[33] Á. Rapp, G. Zaránd, C. Honerkamp, and W. Hofstetter, Phys. Rev. Lett. **98**, 160405 (2007).

[34] C. Honerkamp and W. Hofstetter, Phys. Rev. Lett. **92**, 170403 (2004).

[35] M. Hermele, V. Gurarie, and A. M. Rey, Phys. Rev. Lett. **103**, 135301 (2009).

[36] M. A. Cazalilla, A. F. Ho, and M. Ueda, New J. Phys. **11**, 103033 (2009).

[37] A. V. Gorshkov, M. Hermele, V. Gurarie, C. Xu, P. S. Julienne, J. Ye, P. Zoller, E. Demler, M. D. Lukin, and A. M. Rey, Nat. Phys. **6**, 289 (2010).

[38] S. Taie, Y. Takasu, S. Sugawa, R. Yamazaki, T. Tsujimoto, R. Murakami, and Y. Takahashi, Phys. Rev. Lett. **105**, 190401 (2010).

[39] K. Rodriguez, A. Argüelles, M. Colome-Tatche, T. Vekua, and L. Santos, Phys. Rev. Lett. **105**, 050402 (2010).

[40] See Supplemental Material at http://link.aps.org/supplemental/10.1103/PhysRevLett.110.250402 for details on the quantum gas preparation, detection and data analysis, as well as in-depth discussion of the theoretical model, the method of moments, and the tensor decomposition.

[41] U. Ebling, A. Eckardt, and M. Lewenstein, Phys. Rev. A **84**, 063607 (2011).

[42] Y. Endo and T. Nikuni, J. Low Temp. Phys. **152**, 21 (2008).

[43] S. S. Natu and E. J. Mueller, Phys. Rev. A **81**, 053617 (2010).

[44] The equation is depicted symbolically. For an explicit derivation see [40].

[45] J. M. McGuirk and L. F. Zajiczek, New J. Phys. **12**, 103020 (2010).